Commun. Comput. Phys.
doi: 10.4208/cicp.130411.230911a

Vol. **12**, No. 5, pp. 1329-1358
November 2012

Galerkin-Laguerre Spectral Solution of Self-Similar Boundary Layer Problems

F. Auteri* and L. Quartapelle

Politecnico di Milano, Dipartimento di Ingegneria Aerospaziale,
Via La Masa 34, 20156 Milano, Italy.

Received 13 April 2011; Accepted (in revised version) 23 September 2011

Communicated by Jie Shen

Available online 8 May 2012

Abstract. In this work the Laguerre basis for the biharmonic equation introduced by Jie Shen is employed in the spectral solution of self-similar problems of the boundary layer theory. An original Petrov-Galerkin formulation of the Falkner-Skan equation is presented which is based on a judiciously chosen special basis function to capture the asymptotic behaviour of the unknown. A spectral method of remarkable simplicity is obtained for computing Falkner-Skan-Cooke boundary layer flows. The accuracy and efficiency of the Laguerre spectral approximation is illustrated by determining the linear stability of nonseparated and separated flows according to the Orr-Sommerfeld equation. The pentadiagonal matrices representing the derivative operators are explicitly provided in an Appendix to aid an immediate implementation of the spectral solution algorithms.

AMS subject classifications: 34L16, 34L30, 65L60, 76E05

Key words: Laguerre polynomials, semi-infinite interval, boundary layer theory, Falkner-Skan equation, Cooke equation, Orr-Sommerfeld equation, linear stability of parallel flows.

1 Introduction

The interest in self-similar solutions of the boundary layer equation started in the first half of last century when, a few years after Prandtl formulated the boundary layer equations in 1904, Blasius obtained the ordinary differential equation for the self-similar boundary layer on a flat plate at zero incidence, see [12] and the references therein, and Falkner and Skan [9] derived the general equation for self-similar boundary layers, which is the subject of the present work. Despite such a long history, this problem still collects the interest of researchers and new numerical approaches are tested on it.

*Corresponding author. *Email address:* auteri@aero.polimi.it (F. Auteri)

Two main difficulties have to be faced in the numerical approximation of the Falkner-Skan equation. First, the interval where the solution is sought for is semi-infinite. Second, while conditions on both the unknown and its first derivative supplement the nonlinear differential equation at the wall, at infinity only the first derivative is assigned.

Starting from the early work of Hartree [13], so many different approaches have been proposed to tackle these difficulties that a full account of them would be the subject for a review article and out of the scope of the present paper, so we will provide just a few references. Here, it will suffice to say that two approaches have been mainly adopted to overcome the difficulty arising from the semi-infinite domain: truncation and mapping. After the problem has been reduced to a finite interval problem, the second difficulty can be addressed by solving directly the boundary value problem by means of finite differences [1], finite elements [2] or spectral methods [11]. Alternatively, exploiting shooting methods, the problem can be transformed into an initial value problem, see for instance [5]. A third approach is to restate the problem as a free boundary problem, as first attempted by R. Fazio [10] in the context of self-similar boundary layers and, more recently, by Zhang and Chen [24].

Problems on a semi-infinite domain, however, can be solved without any truncation or rescaling if one introduces Laguerre polynomials/functions [22, 23] or rational functions [4] to build a suitable basis. Recently, Parand and coworkers [17,18] proposed spectral collocation solvers for the Blasius equation which employ Laguerre functions and rational Chebyshev functions, respectively. With respect to truncation methods, these approaches do not require to properly choose the domain size, but allow the user to select spatial resolution of the basis by appropriately selecting a coordinate scaling factor.

While being quite convenient and simple to implement, the collocation approach in spectral methods leads to discrete operators which are full, nonsymmetric, even for self-adjoint problems, and poorly conditioned, especially when high order derivatives are present. On the contrary, in a series of works spanning different coordinate systems and domain geometries, Jie Shen has shown that the spectral Galerkin method can lead to very simple, sparse and optimally conditioned discrete operators. Moreover, the Galerkin method guarantees optimal error estimates. These good properties apply, in particular, to spectral methods on the semi-infinite interval based on Laguerre functions, as shown in [22]. In this work we adopt two different Laguerre spectral bases, both proposed in [22], to solve the Falkner-Skan-Cooke equations and to implement a linear stability solver for both 2D and 3D problems in the parallel flow approximation. By virtue of the adopted bases, boundary conditions are taken into account very easily. Moreover, when discretized, the derivative operators with constant coefficients lead to sparse matrices whose entries have been computed in closed form.

Unfortunately, the Galerkin method can not be applied straightforwardly to solve neither the Blasius nor the Falkner-Skan equation, since Laguerre functions do not satisfy the asymptotic behaviour of the solution, whose limit at infinity is unknown a-priori. To overcome this difficulty, we propose to modify the standard Galerkin method for solutions in L^2 to a Petrov-Galerkin method by resorting to a change of variable and in-

https://doi.org/10.4208/cicp.130411.230911a

troducing a special trial function in the set of the trial functions to properly represent the partially unknown asymptotic behaviour of the solution at infinity. In this way we obtain an elegant, accurate, extremely simple to implement, stable and fast solution algorithm to compute the self-similar boundary layer velocity profiles and to investigate their stability for 2D and 3D flow configurations.

The paper is organized as follows. In the next Section, the Falkner-Skan equations are recalled both in strong form and in weak form. In Section 3, the spectral Laguerre basis for the biharmonic problem is recalled. In Section 4, the Falkner-Skan ordinary differential equation is discretized. In Section 5, a rescaling of the semi-infinite computational domain is introduced which allows to better exploit the proposed basis and results obtained by the present approach are compared with the established literature. In Section 6, the Cooke equation is discretized and some tests are performed. In Section 7, the proposed techniques are applied to the solution of 2D and 3D linear stability problems under the parallel flow assumption. The final section is devoted to some concluding remarks. In the appendix, the coefficients of the constant coefficient linear operators employed throughout the paper are reported in closed form for the first time.

2 Falkner-Skan equation and weak formulation

The Falkner-Skan equation is a third order nonlinear ordinary differential equation which describes the self-similar velocity profile of the boundary layer flow over a wedge, [20],

$$f'''+\alpha ff''+\beta\left[1-(f')^2\right]=0, \tag{2.1}$$

where $f(\eta)$is the unknown while α and β are real constants. For $\beta=0$, the Falkner-Skan equation reduces to the Blasius equation. The Falkner-Skan equation is supplemented by the following boundary conditions:

$$f(0)=0, \qquad f'(0)=0, \qquad \lim_{\eta\to\infty} f'(\eta)=1. \tag{2.2}$$

It should be noted that, for $\beta=0$, the only nonhomogeneity in this problem lies in the third boundary condition as $\eta\to\infty$. The problem is a classical two-point boundary value problem, although the asymptotic condition for $\eta\to\infty$ introduces the difficulty typical of any differential problem over an unbounded domain. This difficulty can be tackled in a spectral context by means of a basis built upon the Laguerre polynomials.

On the other hand, $f'(\infty)=1$ implies the asymptotic behaviour $f(\eta)\to\eta+K$, as $\eta\to\infty$, where K is an unknown constant. Therefore the application of Laguerre polynomials directly to the variable $f(\eta)$ is not possible and one must introduce a new unknown by the following change of variables

$$f(\eta)=\psi(\eta)+\eta\left(1-e^{-\frac{\eta}{2}}\right). \tag{2.3}$$

https://doi.org/10.4208/cicp.130411.230911a

The derivatives of ψ are easily evaluated by a direct calculation which gives

$$f'(\eta)=\psi'(\eta)+1-\left(1-\frac{1}{2}\eta\right)e^{-\frac{\eta}{2}}, \tag{2.4a}$$

$$f''(\eta)=\psi''(\eta)+\left(1-\frac{1}{4}\eta\right)e^{-\frac{\eta}{2}}, \tag{2.4b}$$

$$f'''(\eta)=\psi'''(\eta)-\frac{1}{8}(6-\eta)e^{-\frac{\eta}{2}}. \tag{2.4c}$$

Introducing these expressions in the Falkner-Skan equation (2.1) gives the equation for the new unknown ψ

$$\psi'''+\alpha\psi\psi''-\beta(\psi')^2+\alpha a(\eta)\psi''+\beta b(\eta)\psi'+\alpha c(\eta)\psi=r(\eta), \tag{2.5}$$

where we have introduced the following three shorthands

$$a(\eta)\equiv\eta\left(1-e^{-\frac{\eta}{2}}\right), \tag{2.6a}$$

$$b(\eta)\equiv-2\left[1-\left(1-\frac{1}{2}\eta\right)e^{-\frac{\eta}{2}}\right], \tag{2.6b}$$

$$c(\eta)\equiv\left(1-\frac{1}{4}\eta\right)e^{-\frac{\eta}{2}}, \tag{2.6c}$$

together with a fourth function for the right-hand side

$$r(\eta)\equiv\frac{1}{8}\left[6-\eta+2\alpha(\eta-4)\eta+8\beta(\eta-2)\right]e^{-\frac{\eta}{2}}+\frac{1}{4}\left[\alpha(4-\eta)\eta+\beta(\eta-2)^2\right]e^{-\eta}. \tag{2.7}$$

The boundary conditions supplementing equation (2.5) for the new unknown ψ are fully homogeneous and read

$$\psi(0)=0, \qquad \psi'(0)=0, \qquad \lim_{\eta\to\infty}\psi'(\eta)=0. \tag{2.8}$$

While for $\eta=0$ the boundary conditions on the unknown and its first derivative are homogeneous, asymptotically only the derivatives vanish, since the limit value of the unknown as $\eta\to\infty$ has to be determined in the solution process.

To write Eq. (2.5) in a weak variational form, let us introduce the test function $v(\eta)$ to be defined below, but which is assumed to satisfy the following boundary conditions

$$v(0)=0 \quad \text{and} \quad v(\infty)=0. \tag{2.9}$$

Notice that $v(\eta)$ must be taken to be asymptotically homogeneous to be integrable on the semi-infinite interval.

We first take the inner product of the Eq. (2.5) with the functions v, to obtain

$$\int_0^\infty v(\eta)\left[\psi'''+\alpha\psi\psi''-\beta(\psi')^2+\alpha a(\eta)\psi''+\beta b(\eta)\psi'+\alpha c(\eta)\psi\right]d\eta=\int_0^\infty v(\eta)r(\eta)d\eta. \tag{2.10}$$

https://doi.org/10.4208/cicp.130411.230911a

We now split the integrals of the various terms on the left-hand side and apply the integration by parts to three of them, obtaining

$$\begin{aligned}
&-\int_0^\infty v'(\eta)\psi''d\eta+\left[v(\eta)\psi''\right]_0^\infty-\alpha\int_0^\infty[v(\eta)\psi]'\psi'd\eta+\alpha\left[v(\eta)\psi\psi'\right]_0^\infty\\
&-\beta\int_0^\infty v(\eta)(\psi')^2d\eta-\alpha\int_0^\infty[v(\eta)a(\eta)]'\psi'd\eta+\alpha\left[v(\eta)a(\eta)\psi'\right]_0^\infty\\
&+\beta\int_0^\infty v(\eta)b(\eta)\psi'd\eta+\alpha\int_0^\infty v(\eta)c(\eta)\psi d\eta=\int_0^\infty v(\eta)r(\eta)d\eta.
\end{aligned}$$

Thanks to the boundary conditions (2.9) satisfied by $v(\eta)$, the three boundary terms vanish and the final weak variational equation will be: find $\psi\in\mathcal{K}=\{u(\eta)=k+w(\eta)|k\in\mathbb{R},\ w\in H^2(0,\infty),\ u(0)=u'(0)=0\}$ such that

$$\begin{aligned}
&-\int_0^\infty v'(\eta)\psi''d\eta-\int_0^\infty\left[\alpha v'(\eta)\psi\psi'+(\alpha+\beta)v(\eta)(\psi')^2\right]d\eta\\
&+\int_0^\infty\left\{-\alpha[v(\eta)a(\eta)]'\psi'+\beta v(\eta)b(\eta)\psi'+\alpha v(\eta)c(\eta)\psi\right\}d\eta\\
&=\int_0^\infty v(\eta)r(\eta)d\eta,\qquad\forall v\in H_0^1(0,\infty),
\end{aligned}\tag{2.11}$$

where $H_0^1(0,\infty)=\{v\in H^1(0,\infty),\ v(0)=0\}$. The weak formulation (2.11) is a Petrov-Galerkin method due to the different functional spaces taken for the test and trial functions.

3 Laguerre spectral basis for fourth order problems

To ensure the stability of the discrete approximation of the weak problem, the basis functions for the Galerkin-Laguerre spectral approximation of the biharmonic equation (in one dimension) [22] are considered

$$\mathcal{C}_0(\eta)=e^{-\frac{\eta}{2}},\qquad\mathcal{C}_1(\eta)=\eta e^{-\frac{\eta}{2}},\tag{3.1a}$$

$$\mathcal{C}_i(\eta)=e^{-\frac{\eta}{2}}[L_{i-2}(\eta)-2L_{i-1}(\eta)+L_i(\eta)],\quad i\geq 2.\tag{3.1b}$$

The first two basis functions would enable one to satisfy nonhomogeneous boundary conditions for the unknown variable and its derivative at $\eta=0$. Since $\psi(0)=0$, the first basis function $\mathcal{C}_0(\eta)$ will not be used in the sequel. For $i\geq 2$ the basis functions $\mathcal{C}_i(\eta)$ satisfy homogeneous boundary conditions at $\eta=0$. For this reason, since the solution ψ does not go to zero at infinity but tends to an unknown constant, the biharmonic basis (3.1) must be modified as it will be described in the next section.

It can be proved that

$$\mathcal{C}_i(\eta)=\frac{\eta^2e^{-\frac{\eta}{2}}L_{i-2}^{(2)}(\eta)}{i(i-1)},\qquad i\geq 2.\tag{3.2}$$

https://doi.org/10.4208/cicp.130411.230911a

In fact, let us rewrite the polynomial expression

$$L_{i-2}(\eta)-2L_{i-1}(\eta)+L_i(\eta)=[L_{i-2}(\eta)-L_{i-1}(\eta)]-[L_{i-1}(\eta)-L_i(\eta)] \tag{3.3}$$

and consider the polynomial identity

$$\eta L_{i-1}^{(k+1)}(\eta)=(i+k)L_{i-1}^{(k)}(\eta)-iL_i^{(k)}(\eta), \tag{3.4}$$

which, in the particular case $k=0$, reduces to

$$\eta L_{i-1}^{(1)}(\eta)=i[L_{i-1}(\eta)-L_i(\eta)]. \tag{3.5}$$

Using the latter identity for both terms on the right hand side of relation (3.3), we obtain

$$L_{i-2}(\eta)-2L_{i-1}(\eta)+L_i(\eta)=\frac{\eta}{i(i-1)}\left[iL_{i-2}^{(1)}(\eta)-(i-1)L_{i-1}^{(1)}(\eta)\right]. \tag{3.6}$$

Exploiting one more time the same identity (3.4) but now with $k=1$, we obtain the expression

$$L_{i-2}(\eta)-2L_{i-1}(\eta)+L_i(\eta)=\frac{\eta^2 L_{i-2}^{(2)}(\eta)}{i(i-1)}, \qquad i\geq 2, \tag{3.7}$$

which, after multiplication by $e^{-\frac{\eta}{2}}$, proves (3.2).

4 Laguerre spectral approximation

The functions $\mathcal{C}_i^*(\eta)$, $i=1,2,\cdots$, for the expansion of ψ are identical to those used as test functions, but for the first one. The first test function is

$$\mathcal{C}_1(\eta)=\eta e^{-\frac{\eta}{2}}, \tag{4.1}$$

while the first trial function is chosen to be

$$\mathcal{C}_1^*(\eta)=1-\left(1+\frac{\eta}{2}\right)e^{-\frac{\eta}{2}} \tag{4.2}$$

to satisfy identically all boundary conditions (2.8) on ψ. Then, we assume $\mathcal{C}_i^*(\eta)=\mathcal{C}_i(\eta)$, for any $i\geq 2$. With this assumption we have the expansion

$$\psi(\eta)=\sum_{i=1}^{N}\psi_i\mathcal{C}_i^*(\eta). \tag{4.3}$$

The test functions $\mathcal{C}_i(\eta)$ span the finite dimensional space

$$\mathcal{P}_{0,N}=\left\{v: v=e^{-\frac{\eta}{2}}\eta p(\eta),\ \ p(\eta)\in\mathbb{P}_N(0,\infty)\right\}, \tag{4.4}$$

https://doi.org/10.4208/cicp.130411.230911a

where $\mathbb{P}_N(0,\infty)$ is the space of polynomial functions up to the degree N defined on the semi-infinite interval $[0,\infty)$. The trial functions $\mathcal{C}_i^*(\eta)$ span the finite dimensional space

$$\mathcal{K}_N=\left\{v\colon\ v=\alpha\mathcal{C}_1^*(\eta)+e^{-\frac{\eta}{2}}\eta^2 p(\eta),\ \ \alpha\in\mathbb{R},\ \ p(\eta)\in\mathbb{P}_{N-1}(0,\infty)\right\}. \tag{4.5}$$

Introducing the expansion (4.3) in the weak formulation (2.11) and employing the $\mathcal{C}_i(\eta)$ function as test functions, the discretized Falkner-Skan problem yields the system of nonlinear equations

$$-T^*\boldsymbol{\psi}-\mathbf{nl}(\psi)+(-\alpha A^*+\beta B^*+\alpha C^*)\boldsymbol{\psi}=\boldsymbol{r}. \tag{4.6}$$

The matrix T^* for the third order derivative term, after the integration by parts, has elements given by

$$t_{i,j}^*=\int_0^\infty \mathcal{C}_i'(\eta)\mathcal{C}_j^{*''}(\eta)d\eta,\qquad i,j\geq 1. \tag{4.7}$$

Thus, matrix T^* is obtained by eliminating the first row and column of matrix T, calculated in the Appendix in (A.7), and by evaluating the elements $t_{i,1}^*$ of the (new) first column, to give, for any $i,j\geq 1$,

$$T^*=\frac{1}{8}\begin{pmatrix} 1 & 3 & 1 & & & & \\ \frac{1}{2} & 0 & -2 & -1 & & & \\ \frac{1}{2} & 2 & 0 & -2 & -1 & & \\ & 1 & 2 & \ddots & \ddots & \ddots & \\ & & 1 & \ddots & \ddots & -2 & -1 \\ & & & \ddots & 2 & 0 & -2 \\ & & & & 1 & 2 & 0 \end{pmatrix}. \tag{4.8}$$

The components of the nonlinear term **nl** of the Falkner-Skan equation are

$$\mathrm{nl}_i(\psi)=\int_0^\infty\left[\alpha\mathcal{C}_i'(\eta)\psi\psi'+(\alpha+\beta)\mathcal{C}_i(\eta)(\psi')^2\right]d\eta. \tag{4.9}$$

The elements of matrix A^* corresponding to the third term of the equation are

$$\begin{aligned} a_{i,j}^*&=\int_0^\infty[\mathcal{C}_i(\eta)a(\eta)]'\mathcal{C}_j^{*'}(\eta)d\eta\\ &=\int_0^\infty\left[\mathcal{C}_i'(\eta)a(\eta)+\mathcal{C}_i(\eta)a'(\eta)\right]\mathcal{C}_j^{*'}(\eta)d\eta,\qquad i,j\geq 1. \end{aligned} \tag{4.10}$$

The elements of matrix B^* are defined by

$$b_{i,j}^*=\int_0^\infty\mathcal{C}_i(\eta)b(\eta)\mathcal{C}_j^{*'}(\eta)d\eta,\qquad i,j\geq 1. \tag{4.11}$$

https://doi.org/10.4208/cicp.130411.230911a

Finally, the elements of matrix C^* are

$$c^*_{i,j} = \int_0^\infty \mathcal{C}_i(\eta) c(\eta) \mathcal{C}^*_j(\eta) d\eta, \qquad i,j \geq 1. \tag{4.12}$$

The right-hand side of the nonlinear system is $r_i = \int_0^\infty \mathcal{C}_i(\eta) r(\eta) d\eta$. All the linear terms of the system can be collected together by introducing the matrix $L^* = -T^* - \alpha A^* + \beta B^* + \alpha C^*$, to recast the nonlinear system (4.6) in the form $\boldsymbol{N}(\psi) \equiv L^* \boldsymbol{\psi} - \mathbf{nl}(\psi) - \boldsymbol{r} = 0$. Then the Jacobian matrix for the Newton iteration will be

$$J(\psi) = \frac{\partial \boldsymbol{N}(\psi)}{\partial \boldsymbol{\psi}}. \tag{4.13}$$

The explicit evaluation of the partial derivatives of the nonlinear term (4.9) gives the elements of the Jacobian matrix in the form

$$J_{i,j}(\psi) = \ell^*_{i,j} - \int_0^\infty \left\{ \alpha \mathcal{C}'_i(\eta) \left[\psi'(\eta) \mathcal{C}^*_j(\eta) + \psi(\eta) \mathcal{C}^{*'}_j(\eta) \right] + 2(\alpha+\beta) \mathcal{C}_i(\eta) \psi'(\eta) \mathcal{C}^{*'}_j(\eta) \right\} d\eta, \tag{4.14}$$

where $\ell^*_{i,j} = -t^*_{i,j} - \alpha a^*_{i,j} + \beta b^*_{i,j} + \alpha c^*_{i,j}$. If the Newton method is implemented in incremental form, the variation $\Delta\boldsymbol{\psi}_{k+1} = \boldsymbol{\psi}_{k+1} - \boldsymbol{\psi}_k$ of the unknown at the iteration $k+1$ will be provided by $\Delta\boldsymbol{\psi}_{k+1} = -[J(\psi_k)]^{-1} \boldsymbol{N}(\psi_k)$.

5 Independent variable scaling

To improve the accuracy of the solver, it is useful to properly scale the independent variable. In fact, as the polynomial degree is increased, the approximation resolution is increased mainly far from the wall, where it is less needed. It is then useful to scale the independent variable to improve the resolution near the wall and, eventually, the approximation accuracy.

We introduce then a scaling factor χ and the new variable $\hat{\eta}$ defined as the scaled variable η, namely $\hat{\eta} = \eta/\chi$. By introducing this scaling in the unknown function, we obtain

$$f(\eta) = f(\chi\hat{\eta}) = \hat{f}(\hat{\eta}) = \hat{f}\left(\frac{\eta}{\chi}\right). \tag{5.1}$$

The derivatives of the original unknown function can be computed in terms of the derivatives of the scaled unknown by the chain rule,

$$f'(\eta) = \hat{f}'(\hat{\eta}) \frac{d\hat{\eta}}{d\eta} = \frac{1}{\chi} \hat{f}'(\hat{\eta}), \quad f''(\eta) = \frac{1}{\chi^2} \hat{f}''(\hat{\eta}), \quad f'''(\eta) = \frac{1}{\chi^3} \hat{f}'''(\hat{\eta}). \tag{5.2}$$

Introducing the above substitutions in the Falkner-Skan equation and simplifying we obtain the equation for the scaled unknown

$$\hat{f}''' + \chi\alpha \hat{f} \hat{f}'' + \chi\beta \left[\chi^2 - (\hat{f}')^2 \right] = 0 \tag{5.3}$$

https://doi.org/10.4208/cicp.130411.230911a

supplemented by the three boundary conditions

$$\hat{f}(0)=0, \qquad \hat{f}'(0)=0, \qquad \lim_{\hat{\eta}\to\infty}\hat{f}'(\hat{\eta})=\chi. \tag{5.4}$$

Also in this case, a change of variables is required to accommodate the asymptotic boundary condition for $\hat{f}$ within the framework of the Petrov-Galerkin formulation,

$$\hat{f}(\hat{\eta})=\hat{\psi}(\hat{\eta})+\chi\hat{\eta}\left(1-e^{-\frac{\hat{\eta}}{2}}\right), \tag{5.5}$$

where the χ coefficient in front of the second term on the right hand side should be noted. By virtue of this coefficient, the asymptotic boundary condition is satisfied, provided $\hat{\psi}(\hat{\eta})$ tends to a constant for $\hat{\eta}\to\infty$.

The derivatives of $\hat{f}$ can also be computed

$$\hat{f}'(\hat{\eta})=\hat{\psi}'(\hat{\eta})+\chi\left[1-\left(1-\frac{1}{2}\hat{\eta}\right)e^{-\frac{\hat{\eta}}{2}}\right], \tag{5.6a}$$

$$\hat{f}''(\hat{\eta})=\hat{\psi}''(\hat{\eta})+\chi\left(1-\frac{1}{4}\hat{\eta}\right)e^{-\frac{\hat{\eta}}{2}}, \tag{5.6b}$$

$$\hat{f}'''(\hat{\eta})=\hat{\psi}'''(\hat{\eta})-\frac{1}{8}\chi(6-\hat{\eta})e^{-\frac{\hat{\eta}}{2}}. \tag{5.6c}$$

Substituting these expressions in the scaled Falkner-Skan equation (5.3), the equation for the new unknown $\hat{\psi}$ assumes the form

$$\hat{\psi}'''+\chi\alpha\hat{\psi}\hat{\psi}''-\chi\beta\left(\hat{\psi}'\right)^2+\chi^2\left[\alpha a(\hat{\eta})\hat{\psi}''+\beta b(\hat{\eta})\hat{\psi}'+\alpha c(\hat{\eta})\hat{\psi}\right]=\hat{r}(\hat{\eta}), \tag{5.7}$$

where the functions a, b and c are the same defined for the unscaled problem but are evaluated for the new scaled independent variable $\hat{\eta}$. The new right-hand side is

$$\hat{r}(\hat{\eta})\equiv\frac{1}{8}\chi\left\{6-\hat{\eta}+\chi^2[2\alpha(\hat{\eta}-4)\hat{\eta}+8\beta(\hat{\eta}-2)]\right\}e^{-\frac{\hat{\eta}}{2}}+\frac{1}{4}\chi^3\left[\alpha(4-\hat{\eta})\hat{\eta}+\beta(\hat{\eta}-2)^2\right]e^{-\hat{\eta}}. \tag{5.8}$$

The weak formulation is obtained in the very same way as done before. The nonlinear system of equations of the scaled problem can be written compactly as

$$\hat{L}^*_\chi\hat{\boldsymbol{\psi}}-\chi\mathbf{nl}(\hat{\psi})=\hat{\boldsymbol{r}}, \tag{5.9}$$

where the matrix of the linear part of the scaled equation $\hat{L}^*_\chi\equiv-T^*+\chi^2(-\alpha A^*+\beta B^*+\alpha C^*)$ has been introduced and where $\hat{r}_i=\int_0^\infty C_i(\hat{\eta})\hat{r}(\hat{\eta})d\hat{\eta}$, for $i=1,2,\cdots$.

5.1 Results

To assess the accuracy properties of the proposed method, present results are compared with reference values provided in the literature. In particular, for the Blasius equation ($\alpha=0.5$ and $\beta=0$), the most accurate solutions to date were those obtained by a Laguerre

Table 1: Blasius equation, $f''(0)$ value. Comparison of present result without scaling (second column), with scaling factor $\chi=0.1$ (third column) with the values from [18] (last column). The reference value is 0.3320573362 from [10], as reported in [3].

N	Present	Present $\chi=0.1$	see [18]
8	0.3483630118	0.4700048153	0.332061648
10	0.3398081761	0.3812924020	0.332058234
12	0.3290996249	0.3434963326	0.332057001
19	0.3335549762	0.3320575807	0.332057314
33	0.3321517910	0.3320573362	0.332057334
64	0.3320554809	0.3320573362	–

Table 2: Falkner-Skan equation, $f''(0)$ value. Comparison of present result for $\alpha=1$ and several values of β with the reference values from [19] and [3]. Spectral resolution $N=64$. Second column: no scaling. Third column: scaling factor $\chi=0.1$. The apex ^{r} indicates the reversed flow cases.

β	Present	Present $\chi=0.1$	see [19]	see [3]
2	1.687217	1.687218169	1.687218	1.687218
1	1.232587	1.232587657	1.232588	1.232589
0.5	0.927686	0.927680040	0.927680	0.927680
-0.1	0.319223	0.319269760	0.319270	0.319270
-0.15	0.216381	0.216361406	0.216362	0.216361
-0.18	0.128778	0.128636221	0.128638	0.128637
-0.1988	0.007870	0.005218188	0.005226	0.005225
-0.18^r	-0.097915	-0.097692060	–	–
-0.15^r	-0.132795	-0.133421238	–	–
-0.1^r	-0.141544	-0.140546213	–	–

collocation method in [18], which reports values obtained with different scalings depending on the number of points. For $N=33$ the present Petrov-Galerkin method provides two more significant digits, as shown in Table 1.

Concerning the solution of the Falkner-Skan equations, we compare our results with those reported in [19] and [3] in Table 2. Results are calculated for $\alpha=1$ both without scaling and with scaling factor $\chi=0.1$. While the former do not achieve a notable degree of accuracy, the latter can provide up to 10 exact significant digits, improving considerably the existent results reported in the literature. The last three rows of the same table report $f''(0)$ for the reversed flow for three different values of β. For the flows with $\beta=-0.18$, our solutions provide the $f''(0)$ with an additional significant figure with respect to the result $f''(0)=-0.09769206$ reported in [14].

6 Cooke equation

The Falkner-Skan solution for a two-dimensional boundary layer on a wedge has been extended to 3D by Cooke [6] to represent the boundary layer on a swept wedge, see also Appendix B in [7].

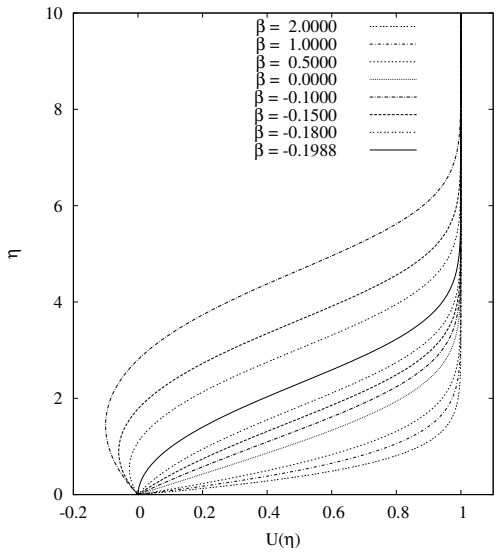

Figure 1: Falkner-Skan velocity profiles for different values of the β parameter and $\alpha=1$.

A further equation is added to the Falkner-Skan one, which describes the behaviour of the z component of the velocity in nondimensional form $g(\eta)=w(\eta)/\lim_{\eta\to\infty}w(\eta)$,

$$g''+\alpha f(\eta)g'=0, \tag{6.1}$$

supplemented by the boundary conditions

$$g(0)=0 \quad \text{and} \quad \lim_{\eta\to\infty} g(\eta)=1. \tag{6.2}$$

Before discretizing the Cooke equation it is necessary to relieve the non-homogeneous asymptotic condition. Let us introduce the following change of variables:

$$g(\eta)=\gamma(\eta)+1-e^{-\frac{\eta}{2}}, \tag{6.3}$$

the auxiliary unknown satisfies homogeneous asymptotic conditions and can be therefore discretized directly by generalized Laguerre functions. The first and second derivatives of the unknown function can be immediately computed

$$g'(\eta)=\gamma'(\eta)+\frac{1}{2}e^{-\frac{\eta}{2}}, \qquad g''(\eta)=\gamma''(\eta)-\frac{1}{4}e^{-\frac{\eta}{2}}. \tag{6.4}$$

Introducing the change of variables in the Cooke equation, we obtain

$$\gamma''+\alpha f(\eta)\gamma'=h(\eta), \tag{6.5}$$

where $h(\eta)\equiv\frac{1}{4}[1-2\alpha f(\eta)]e^{-\frac{\eta}{2}}$.

A Galerkin discretization can be envisaged for this equation. Let us consider the following generalized Laguerre functions as basis functions:

$$\mathcal{B}_i(\eta) \equiv \frac{\eta e^{-\frac{\eta}{2}} L_{i-1}^{(1)}(\eta)}{i}, \quad \text{for } i \geq 1, \tag{6.6}$$

the expansion for the auxiliary unknown $\gamma(\eta)$ which automatically satisfies the boundary and asymptotic conditions will read

$$\gamma(\eta) = \sum_{i=1}^{I} \gamma_i \mathcal{B}_i(\eta). \tag{6.7}$$

The equation can be rewritten in weak form by taking the inner-product, in the L^2 sense, of the equation with the basis functions themselves. Integrating by parts the first term, since the basis functions annihilate at the extremes, we obtain, for all $1 \leq i \leq I$,

$$\sum_{j=1}^{I} \Big[-\int_0^\infty \mathcal{B}_i'(\eta)\mathcal{B}_j'(\eta)d\eta + \alpha \int_0^\infty \mathcal{B}_i(\eta) f(\eta) \mathcal{B}_j'(\eta) d\eta \Big] \gamma_j = \int_0^\infty \mathcal{B}_i(\eta) h(\eta) d\eta, \tag{6.8}$$

which can be put in the following matrix form

$$\big(-\tilde{D}^2 + \alpha \tilde{F}\big)\boldsymbol{\gamma} = \boldsymbol{h}, \tag{6.9}$$

where $\tilde{D}^2$ is the stiffness matrix, after the integration by parts, in the basis $\mathcal{B}_i(\eta)$, with elements defined by

$$\tilde{d}^2_{i,j} = \int_0^\infty \mathcal{B}_i'(\eta)\mathcal{B}_j'(\eta)d\eta, \qquad i,j \geq 1. \tag{6.10}$$

Matrix $\tilde{D}^2$ is tridiagonal and its elements can be computed in closed form, see the appendix,

$$\tilde{D}^2 = \frac{1}{4} \begin{pmatrix} 2 & 1 & & & & \\ 1 & 2 & 1 & & & \\ & 1 & \ddots & \ddots & & \\ & & \ddots & \ddots & \ddots & \\ & & & \ddots & \ddots & 1 \\ & & & & 1 & 2 \end{pmatrix}. \tag{6.11}$$

The matrix $\tilde{F}$ is full and its elements are defined as

$$\tilde{f}_{i,j} = \int_0^\infty \mathcal{B}_i(\eta) f(\eta) \mathcal{B}_j'(\eta) d\eta, \qquad i,j \geq 1. \tag{6.12}$$

The components of the right-hand side $\boldsymbol{h}$ are defined as

$$h_i = \int_0^\infty \mathcal{B}_i(\eta) h(\eta) d\eta, \qquad i \geq 1. \tag{6.13}$$

The Cooke equation is linear and can be readily solved once the solution $f(\eta)$ of the Falkner-Skan equation has been determined.

6.1 Results

In Table 3 we report the value of $g'(0)$ for several values of the β parameter in the Falkner-Skan-Cooke equations. All reported values have been computed for $\alpha=1$ and $N=64$. To obtain the tenth exact significant figure also for $\beta=-0.1988$ and for two reverse flow solutions with $\beta=-0.18$ and $\beta=-0.15$, the spatial resolution must be increased. For $N=128$ and $\chi=0.1$ we find $g'(0)=0.3285663718$, 0.2557614367 and 0.2030896681, respectively.

Table 3: Falkner-Skan equation, $g'(0)$ value. Comparison of present result for several values of β and $N=64$ without scaling (second column), with scaling factor $\chi=0.1$ (third column). The apex ^{r} indicates the reversed flow cases.

β	$g'(0)$	$g'(0), \chi=0.1$
2	0.60521	0.6051972393
1	0.57048	0.5704652525
0.5	0.53899	0.5389789351
-0.1	0.43675	0.4367975316
-0.15	0.40931	0.4093363120
-0.18	0.38117	0.3811240379
-0.1988	0.33004	0.328566372
-0.18^r	0.25560	0.255761437
-0.15^r	0.20342	0.203089668
-0.1^r	0.13052	0.1315065229

Moreover, in Fig. 2 the $w(\eta)$ profiles are shown for the same values of the parameter β reported in the table. Please note that two different profiles are plotted for negative values of β, since both the attached solution and the reverse flow solution have been provided, with an inflection point occurring only in the latter.

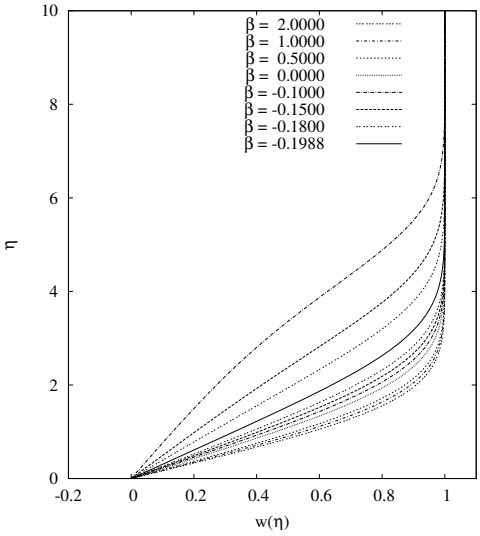

Figure 2: Cooke velocity profiles for different values of the β parameter and $\alpha=1$.

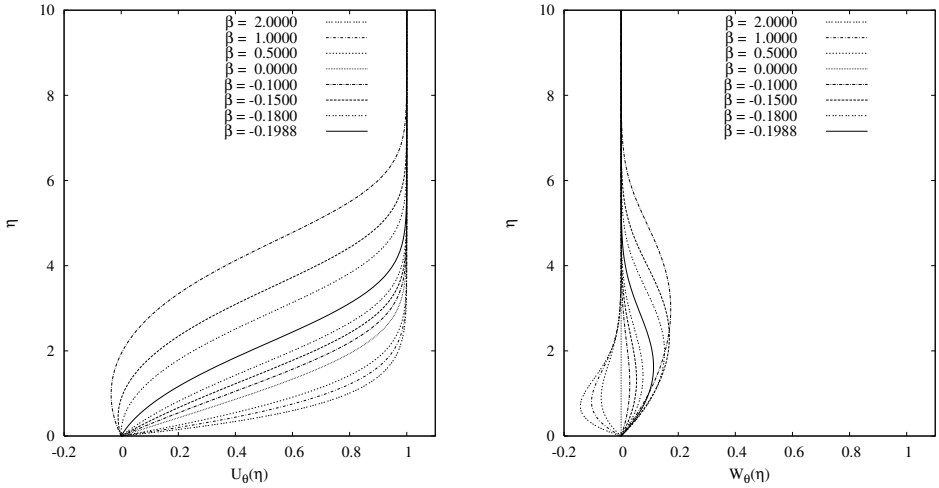

Figure 3: Velocity profiles of the Falkner-Skan-Cooke swept boundary layer for $\theta = 30^\circ$ in a coordinate system aligned with the free stream velocity. Left: longitudinal component. Right: transverse component.

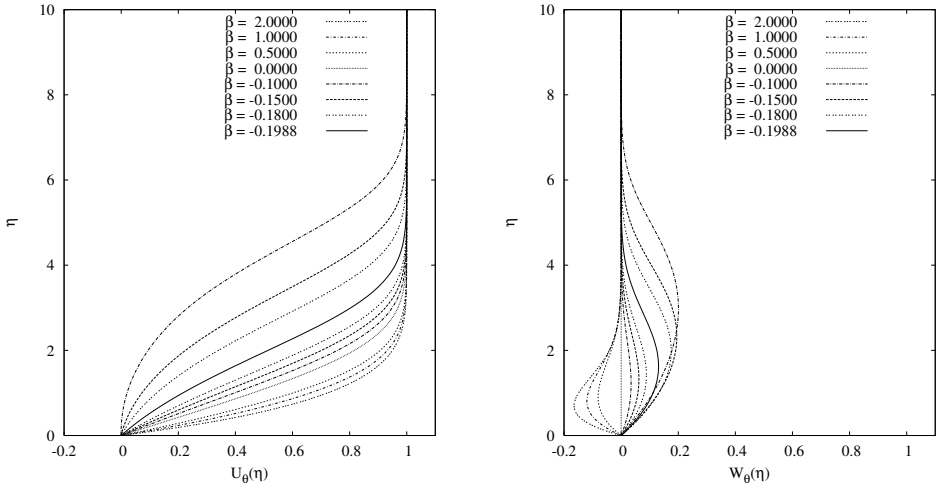

Figure 4: Velocity profiles of the Falkner-Skan-Cooke swept boundary layer for $\theta = 45^\circ$ in a coordinate system aligned with the free stream velocity. Left: longitudinal component. Right: transverse component.

Finally, it is also interesting to show the velocity profiles in a coordinate system with an axis parallel to the external flow, and the other axis perpendicular to it. This is especially interesting to highlight the inflection point which is present in the traverse velocity profile, which severely affects the stability of the boundary layer. Let us denote by U_e and W_e the velocity components of the external velocity in a Cartesian frame such that the external velocity $\boldsymbol{U}_e = U_e\hat{\boldsymbol{x}} + W_e\hat{\boldsymbol{z}}$ is a function of the x coordinate only. A new reference frame is introduced which is rotated by the angle $\theta = \tan^{-1}(W_e/U_e)$ with respect to the original Cartesian frame. The velocity components in this rotated frame are denoted by

$U_\theta(\eta)$ and $W_\theta(\eta)$. They are obtained from $U(\eta)$ and $W(\eta)$ by the transformation matrix of the axis rotation, to give

$$U_\theta(\eta)=|\boldsymbol{U}_\mathrm{e}|\left[\cos^2\theta f'(\eta)+\sin^2\theta g(\eta)\right], \qquad W_\theta(\eta)=|\boldsymbol{U}_\mathrm{e}|\sin\theta\cos\theta[-f'(\eta)+g(\eta)]. \quad (6.14)$$

In Fig. 3 the streamwise and transverse components of the velocity profile in the Falkner-Skan-Cooke boundary layer are provided for a sweep angle $\theta=30^\circ$. In the next figure, Fig. 4, the analogous profiles are given for a sweep angle $\theta=45^\circ$ which is characterized by the maximum transverse velocity for fixed β, see e.g., [15].

7 Linear stability for unbounded parallel flows

7.1 Two-dimensional disturbances: Orr-Sommerfeld equation

Let us consider a planar steady flow with velocity $U(y)$, $\hat{\boldsymbol{x}}$ parallel to a horizontal wall at $y=0$ and a wave-like, two-dimensional perturbation

$$\psi_\mathrm{perturb}(\xi,\eta,\tau)=\phi(\eta)e^{\mathrm{i}\,\alpha(\xi-c\tau)}, \quad (7.1)$$

where all variables are dimensionless and defined as follows

$$\xi=\frac{x}{G(\bar{x})}, \qquad \eta=\frac{y}{G(\bar{x})}, \qquad \tau=\frac{tU_\mathrm{e}}{G(\bar{x})}, \quad (7.2)$$

with $G(x)$ denoting a generic boundary layer thickness. In the perturbation expression (7.1) the dimensionless wavenumber variable α should not be confused with the parameter of the Falkner-Skan equation. The dimensionless phase velocity c has to be determined by solving the generalized eigenvalue problem, to locate the most unstable mode as a function of the dimensionless wavenumber α and of the Reynolds number defined by

$$\mathrm{Re}=\frac{U_\mathrm{e}G(\bar{x})}{\nu}. \quad (7.3)$$

The equation governing the wave-like perturbation is the celebrated Orr-Sommerfeld equation

$$\frac{1}{\mathrm{Re}}(\phi''''-2\alpha^2\phi''+\alpha^4\phi)+\mathrm{i}\alpha[\mathcal{U}(\eta)-c]\left(-\phi''+\alpha^2\phi\right)+\mathrm{i}\alpha\mathcal{U}''(\eta)\phi=0, \quad (7.4)$$

where $\mathcal{U}=U/U_\mathrm{e}$ is the dimensionless base flow velocity and the prime denotes differentiation with respect to the dimensionless wall normal coordinate η. The equation is supplemented by the homogeneous boundary conditions

$$\phi(0)=\phi'(0)=\phi(\infty)=\phi'(\infty)=0. \quad (7.5)$$

A couple of observations are in order. First, the Orr-Sommerfeld equation assumes the base flow to be parallel. In general this is not the case for a boundary layer flow, since the

boundary layer thickness grows with the spatial coordinate x. However, the parallel Orr-Sommerfeld problem can be viewed as the zero order approximation to the non-parallel linear stability problem when a multiple scale expansion is employed. Second, it is to be emphasized that the previous equation has been made nondimensional employing, as local reference length, the function $G(x)$ which is proportional to the local boundary layer thickness. Hence, all constants, i.e., Re, α, and c, and the dependent variable η are referred to such function $G(x)$. In the literature, however, results are often referred to the boundary layer displacement thickness $\delta_1(x)$, which is proportional to $G(x)$. In this case a simple scaling of the relevant quantities allows one to compare results. In fact, let us consider the Reynolds number:

$$\mathrm{Re}_1 = \frac{U_e \delta_1(\bar{x})}{\nu} = \mathrm{Re}\frac{\delta_1(\bar{x})}{G(\bar{x})}, \tag{7.6}$$

where, since $U(y)/U_e = \mathcal{U}(\eta) = f'(\eta)$, the ratio

$$\frac{\delta_1(\bar{x})}{G(\bar{x})} = \int_0^\infty [1-\mathcal{U}(\eta)]d\eta = \lim_{\eta\to\infty}[\eta - f(\eta)] = -\lim_{\eta\to\infty}\psi(\eta) = -\psi_1 \tag{7.7}$$

is a constant, not depending on $\bar{x}$, in a similitude boundary layer. It can be noted in passing that, for the Blasius problem, the first expansion coefficient ψ_1 is related to the constant b_1 occurring in the asymptotic expansion of the solution as $\eta \to \infty$ [16, pp. 105] given by

$$f_{\mathrm{Blasius}}(\eta) \sim \eta - b_1 + b_2 \int_\eta^\infty d\sigma \int_\sigma^\infty e^{-\frac{(\lambda-b_1)^2}{4}} d\lambda + \cdots \tag{7.8}$$

with b_2 denoting another constant and $b_1 = -\psi_1 = 1.72078765752$.

In general, for the Falkner-Skan solution, we have

$$\mathrm{Re} = \mathrm{Re}_1 \frac{G(\bar{x})}{\delta_1(\bar{x})} = \frac{\mathrm{Re}_1}{|\psi_1|}. \tag{7.9}$$

Similarly,

$$\frac{\alpha_1}{\delta_1(\bar{x})} = \frac{\alpha}{G(\bar{x})} \Rightarrow \alpha = \alpha_1 \frac{G(\bar{x})}{\delta_1(\bar{x})} = \frac{\alpha_1}{|\psi_1|} \tag{7.10}$$

and

$$c_1 \delta_1(\bar{x}) = c G(\bar{x}) \Rightarrow c_1 = c \frac{G(\bar{x})}{\delta_1(\bar{x})} = \frac{c}{|\psi_1|}. \tag{7.11}$$

Now, by separating the part containing the eigenvalue and regrouping some terms, the Orr-Sommerfeld equation becomes

$$\phi'''' - 2\alpha^2\phi'' + \alpha^4\phi + \mathrm{i}\alpha\mathrm{Re}\{-[\mathcal{U}(\eta)\phi' - \mathcal{U}'(\eta)\phi]' + \alpha^2\mathcal{U}(\eta)\phi\} = \mathrm{i}c\alpha\mathrm{Re}(-\phi'' + \alpha^2\phi). \tag{7.12}$$

https://doi.org/10.4208/cicp.130411.230911a

The weak variational form of the problem is obtained by multiplying the equation by a test function $v(\eta)$ satisfying the two conditions $v(0)=0$ and $v'(0)=0$ and integrating all terms of the equation. The eigenfunction $\phi(\eta)$ is expanded as follows

$$\phi(\eta)=\sum_{i=2}^{I}\phi_i\mathcal{C}_i(\eta) \tag{7.13}$$

and the test function is taken as $v(\eta)=\mathcal{C}_i(\eta)$. In the weak equation, the term with the fourth order derivative and all those with a second order derivative are integrated by parts. The velocity $\mathcal{U}$ of the parallel base flow is expressed by $\mathcal{U}=f'$, with f solution to the Falkner-Skan equation. This means that $f(\eta)=\psi(\eta)+\eta(1-e^{-\eta/2})$, with $\psi(\eta)$ given by the expansion (4.3) and solution to the nonlinear system (4.6). This leads to the discrete eigenvalue problem

$$\left[D^4+2\alpha^2D^2+\alpha^4M+\mathrm{i}\alpha\mathrm{Re}\left(N+\alpha^2U\right)\right]\boldsymbol{\phi}=\mathrm{i}c\alpha\mathrm{Re}\left(D^2+\alpha^2M\right)\boldsymbol{\phi}. \tag{7.14}$$

Here M, D^2 and D^4 denote the square matrices with elements defined by $m_{i,j}=\int_0^\infty\mathcal{C}_i(\eta)\mathcal{C}_j(\eta)d\eta$, $d^2_{i,j}=\int_0^\infty\mathcal{C}_i'(\eta)\mathcal{C}_j'(\eta)d\eta$ and $d^4_{i,j}=\int_0^\infty\mathcal{C}_i''(\eta)\mathcal{C}_j''(\eta)d\eta$, with $i,j\geq 2$. They are obtained from the complete matrices introduced in the Appendix, which account also for the first two modes corresponding to $i=0$ and $i=1$, by eliminating the first two rows and two columns. Moreover, U and N denote the square matrices with elements defined respectively by

$$u_{i,j}=\int_0^\infty\mathcal{C}_i(\eta)f'(\eta)\mathcal{C}_j(\eta)d\eta, \qquad i,j\geq 2, \tag{7.15a}$$

$$n_{i,j}=\int_0^\infty\mathcal{C}_i'(\eta)\left[f'(\eta)\mathcal{C}_j'(\eta)-f''(\eta)\mathcal{C}_j(\eta)\right]d\eta, \qquad i,j\geq 2. \tag{7.15b}$$

We note the particular form of the expression of the term $\left[\mathcal{U}'(\eta)\phi\right]'$ in the Orr-Sommerfeld equation (7.12). This form is crucial to avoid, jointly with the integration by parts, the explicit evaluation of the second derivative U'' which otherwise "must be known accurately", as pointed out in [20, pp. 434]. On the other hand, the use of the biharmonic basis $\mathcal{C}_i(\eta)$ in the solution of the Falkner-Skan equation, guarantees a computation of $\mathcal{U}'=f''$ with the required accuracy.

The generalized complex eigenvalue problem (7.14) can be written compactly as

$$A(\alpha,\mathrm{Re})\boldsymbol{\phi}=cB(\alpha,\mathrm{Re})\boldsymbol{\phi}, \tag{7.16}$$

where

$$A(\alpha,\mathrm{Re})=D^4+2\alpha^2D^2+\alpha^4M+\mathrm{i}\alpha\mathrm{Re}\left(N+\alpha^2U\right), \quad B(\alpha,\mathrm{Re})=\mathrm{i}\alpha\mathrm{Re}\left(D^2+\alpha^2M\right). \tag{7.17}$$

The complex eigenvalue $c=c_\mathrm{r}+\mathrm{i}c_\mathrm{i}$ will depend on α and Re, namely: $c=c_\mathrm{r}(\alpha,\mathrm{Re})+\mathrm{i}c_\mathrm{i}(\alpha,\mathrm{Re})$. The Orr-Sommerfeld problem can be also recast in scaled form and the corresponding equation for the unknown $\hat{\phi}(\hat{\eta})=\phi(\chi\hat{\eta})=\phi(\eta)$ would be

$$\begin{aligned}\hat{\phi}''''-2\hat{\alpha}^2\hat{\phi}''+\hat{\alpha}^4\hat{\phi}+\mathrm{i}\chi\hat{\alpha}\mathrm{Re}\left\{-\left[\hat{\mathcal{U}}(\hat{\eta})\hat{\phi}'-\hat{\mathcal{U}}'(\hat{\eta})\hat{\phi}\right]'+\hat{\alpha}^2\hat{\mathcal{U}}(\hat{\eta})\hat{\phi}\right\}\\ =\mathrm{i}\hat{c}\hat{\alpha}\mathrm{Re}\left(-\hat{\phi}''+\hat{\alpha}^2\hat{\phi}\right),\end{aligned} \tag{7.18}$$

https://doi.org/10.4208/cicp.130411.230911a

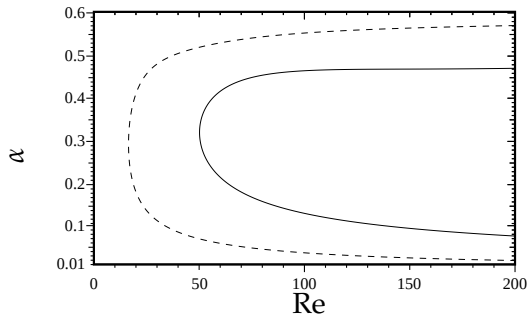

Figure 5: Neutral stability curves for two different Falkner-Skan boundary layers. Solid line: decelerating, nonseparated, boundary layer with $\alpha_{\rm FS}=1$, $\beta_{\rm FS}=-0.18$. Dashed line: decelerating, separated, boundary layer with $\alpha_{\rm FS}=1$, $\beta_{\rm FS}=-0.18$.

where the prime acting on $\hat{\phi}$ denotes differentiation with respect to the new variable $\hat{\eta}$, $\hat{\mathcal{U}}(\hat{\eta})=\mathcal{U}(\chi\hat{\eta})$ and $\hat{\mathcal{U}}'(\hat{\eta})=\chi\mathcal{U}'(\chi\hat{\eta})$, and also $\hat{\alpha}=\chi\alpha$ and $c=\hat{c}/\chi$. In terms of the original solution $f(\eta)$ to the *unscaled* Falkner-Skan equation (2.1), the scaled Orr-Sommerfeld equation reads

$$\begin{aligned}\hat{\phi}''''-2\hat{\alpha}^2\hat{\phi}''+\hat{\alpha}^4\hat{\phi}+\mathrm{i}\hat{\alpha}\mathrm{Re}\{-\left[\chi f'(\chi\hat{\eta})\hat{\phi}'-\chi^2 f''(\chi\hat{\eta})\hat{\phi}\right]'+\hat{\alpha}^2\chi f'(\chi\hat{\eta})\hat{\phi}\}\\ =\mathrm{i}\hat{c}\hat{\alpha}\mathrm{Re}\left(-\hat{\phi}''+\hat{\alpha}^2\hat{\phi}\right).\end{aligned} \tag{7.19}$$

As a test case, we calculated the neutral stability curves for to two decelerating Falkner-Skan boundary layers, both for $\alpha_{\rm FS}=1$, $\beta_{\rm FS}=-0.18$. The results are reported in Fig. 5, that are in excellent agreement with the analogous figure reported in [14].

7.2 Three-dimensional disturbances: Orr-Sommerfeld-Squire system

We now consider three-dimensional disturbances of the normal velocity consisting in plane waves propagating parallel to the plane wall:

$$v(\xi,\eta,\zeta,\tau)=v(\eta)e^{\mathrm{i}\,(\alpha\xi+\beta\zeta-\alpha c\tau)}, \tag{7.20}$$

where $\zeta=z/g(\bar{x})$. Again, the wavenumber variables α and β here should not be confused with the constant parameters occurring in the Falkner-Skan equation. By a direct calculation the problem for the linear stability of the 3D perturbations assumes the form of a system for the normal components of velocity $v=u_n=u_y$ and vorticity $\omega=\omega_n=\omega_y$, see e.g., [21, pp. 57]:

$$\begin{cases}\dfrac{1}{\mathrm{Re}}\left(v''''-2\alpha_\diamond^2 v''+\alpha_\diamond^4 v\right)-\mathrm{i}\alpha\left[\mathcal{U}(\eta)v'-\mathcal{U}'(\eta)v\right]'+\mathrm{i}\alpha\alpha_\diamond^2\mathcal{U}(\eta)v=\mathrm{i}c\alpha\left(-v''+\alpha_\diamond^2 v\right),\\ \dfrac{1}{\mathrm{Re}}\left(-\omega''+\alpha_\diamond^2\omega\right)+\mathrm{i}\alpha\mathcal{U}(\eta)\omega=\mathrm{i}c\alpha\omega-\mathrm{i}\beta\mathcal{U}'(\eta)v,\end{cases} \tag{7.21}$$

where $\alpha_\diamond^2=\alpha^2+\beta^2$ and where the terms containing the eigenvalue of the temporal problem have been written on the right hand side. The boundary conditions for the variables v

https://doi.org/10.4208/cicp.130411.230911a

and ω are $v(0)=v'(0)=v(\infty)=v'(\infty)=0$ and $\omega(0)=\omega(\infty)=0$. Thanks to Squire's theorem, see e.g., [21], the transversal disturbances do not modify the linear stability of the Falkner-Skan flows. However, the preceding equations have been presented since they represent a step necessary to study the linear stability of the boundary layer with crossflow component solution to the Cooke equation, as described below.

7.3 Stability of Falkner-Skan-Cooke flow

Consider now the three-dimensional boundary layer in which the direction of the mean flow parallel to the wall depends on the normal coordinate. We assume that the spanwise velocity component is the solution to the Cooke equation and that the velocity is described in the rotated Cartesian frame so that $\boldsymbol{U}(\eta)=U_\theta(\eta)\hat{\boldsymbol{x}}+W_\theta(\eta)\hat{\boldsymbol{z}}$, with the two components defined in (6.14), independent of x and z. The adimensionalization of the problem is based on the modulus of the external velocity, namely $|\boldsymbol{U}_\mathrm{e}|=\sqrt{U_\mathrm{e}^2+W_\mathrm{e}^2}$.

The equations for the linear stability analysis of the 3D perturbations $v(\xi,\eta,\zeta,\tau)=v(\eta)e^{\mathrm{i}(\alpha\xi+\beta\zeta-\alpha c\tau)}$ in the rotated reference frame, with the x axis aligned with the direction of the external velocity can be written by introducing the scaled Reynolds number

$$\mathrm{Re}_{1,\theta}=\frac{|\boldsymbol{U}_\mathrm{e}|\delta_1}{\nu}=\frac{U_\mathrm{e}\delta_1}{\nu\cos\theta}=\frac{\mathrm{Re}_1}{\cos\theta}=\frac{|\psi_1|}{\cos\theta}\mathrm{Re}=\mathrm{Re}_\theta|\psi_1|, \tag{7.22}$$

with $\mathrm{Re}_\theta=\mathrm{Re}/\cos\theta$, and by defining the two functions, thanks to (6.14),

$$\begin{aligned}\mathcal{S}_\theta(\eta,\boldsymbol{\alpha}_\diamond)&=\alpha\mathcal{U}_\theta(\eta)+\beta\mathcal{W}_\theta(\eta)\\&=\alpha\left[\cos^2\theta f'(\eta)+\sin^2\theta g(\eta)\right]+\beta\sin\theta\cos\theta[-f'(\eta)+g(\eta)]\end{aligned} \tag{7.23}$$

and

$$\begin{aligned}\mathcal{R}_\theta(\eta,\boldsymbol{\alpha}_\diamond)&=-\beta\mathcal{U}_\theta(\eta)+\alpha\mathcal{W}_\theta(\eta)\\&=-\beta\left[\cos^2\theta f'(\eta)+\sin^2\theta g(\eta)\right]+\alpha\sin\theta\cos\theta[-f'(\eta)+g(\eta)],\end{aligned} \tag{7.24}$$

where $\boldsymbol{\alpha}_\diamond=\alpha\hat{\boldsymbol{x}}+\beta\hat{\boldsymbol{z}}$ is the wave vector in the plane of the plate. The Orr-Sommerfeld-Squire equations for the linear stability of the solution to the Falkner-Skan-Cooke equations are

$$\begin{cases}\dfrac{1}{\mathrm{Re}_\theta}(v''''-2\alpha_\diamond^2v''+\alpha_\diamond^4v)-\mathrm{i}\dfrac{\partial}{\partial\eta}\left[\mathcal{S}_\theta(\eta,\boldsymbol{\alpha}_\diamond)v'-\dfrac{\partial\mathcal{S}_\theta(\eta,\boldsymbol{\alpha}_\diamond)}{\partial\eta}v\right]+\mathrm{i}\alpha_\diamond^2\mathcal{S}_\theta(\eta,\boldsymbol{\alpha}_\diamond)v=\mathrm{i}c\alpha\left(-v''+\alpha_\diamond^2v\right),\\ \dfrac{1}{\mathrm{Re}_\theta}(-\omega''+\alpha_\diamond^2\omega)+\mathrm{i}\mathcal{S}_\theta(\eta,\boldsymbol{\alpha}_\diamond)\omega=\mathrm{i}c\alpha\omega+\mathrm{i}\dfrac{\partial\mathcal{R}_\theta(\eta,\boldsymbol{\alpha}_\diamond)}{\partial\eta}v,\end{cases} \tag{7.25}$$

where $\partial_\eta\mathcal{S}_\theta(\eta,\boldsymbol{\alpha}_\diamond)=\alpha\mathcal{U}_\theta'(\eta)+\beta\mathcal{W}_\theta'(\eta)$. The Orr-Sommerfeld-Squire system can be discretized by introducing the following expansion of the unknowns

$$v(\eta)=\sum_{i=2}^{I}v_i\mathcal{C}_i(\eta)\quad\text{and}\quad\omega(\eta)=\sum_{i=1}^{I}\omega_i\mathcal{B}_i(\eta). \tag{7.26}$$

https://doi.org/10.4208/cicp.130411.230911a

To implicitly satisfy boundary conditions, the expansion for v is the same as that for ϕ in (7.13) and the expansion for ω is the same as that for γ in (6.7). Employing the same basis functions $\mathcal{C}_i(\eta)$ and $\mathcal{B}_i(\eta)$ as test functions, the Galerkin formulation of the two Eqs. (7.25) leads to the two algebraic eigenvalue problems

$$A(\boldsymbol{\alpha}_\diamond,\mathrm{Re}_\theta)\boldsymbol{v}=cB(\boldsymbol{\alpha}_\diamond,\mathrm{Re}_\theta)\boldsymbol{v},\qquad \tilde{A}(\boldsymbol{\alpha}_\diamond,\mathrm{Re}_\theta)\boldsymbol{\omega}=c\tilde{B}(\alpha,\mathrm{Re}_\theta)\boldsymbol{\omega} \tag{7.27}$$

involving the two pairs of matrices

$$A(\boldsymbol{\alpha}_\diamond,\mathrm{Re}_\theta)=D^4+2\alpha_\diamond^2D^2+\alpha_\diamond^4M+\mathrm{i}\mathrm{Re}_\theta\left[N_\theta(\boldsymbol{\alpha}_\diamond)+\alpha_\diamond^2S_\theta(\boldsymbol{\alpha}_\diamond)\right], \tag{7.28a}$$

$$B(\boldsymbol{\alpha}_\diamond,\mathrm{Re}_\theta)=\mathrm{i}\alpha\mathrm{Re}_\theta\left(D^2+\alpha_\diamond^2M\right) \tag{7.28b}$$

and

$$\tilde{A}(\boldsymbol{\alpha}_\diamond,\mathrm{Re}_\theta)=\tilde{D}^2+\alpha_\diamond^2\tilde{M}+\mathrm{i}\mathrm{Re}_\theta\tilde{S}_\theta(\boldsymbol{\alpha}_\diamond), \tag{7.29a}$$

$$\tilde{B}(\alpha,\mathrm{Re}_\theta)=\mathrm{i}\alpha\mathrm{Re}_\theta\tilde{M}. \tag{7.29b}$$

The matrices M, D^2, D^4 are the same as in the two-dimensional problem, the matrix $\tilde{D}^2$ has already been given in (6.11), $\tilde{M}$ has elements $\tilde{m}_{i,j}=\int_0^\infty\mathcal{B}_i(\eta)\mathcal{B}_j(\eta)d\eta$, $i,j\geq1$ given by

$$\tilde{M}=\begin{pmatrix}2&-1&&&\\-1&2&-1&&\\&-1&\ddots&\ddots&\\&&\ddots&\ddots&-1\\&&&-1&2\end{pmatrix}. \tag{7.30}$$

Finally the matrices $S_\theta(\boldsymbol{\alpha}_\diamond)$, $N_\theta(\boldsymbol{\alpha}_\diamond)$ and $\tilde{S}_\theta(\boldsymbol{\alpha}_\diamond)$ have elements defined as follows

$$s^\theta_{i,j}(\boldsymbol{\alpha}_\diamond)=\int_0^\infty\mathcal{C}_i(\eta)\mathcal{S}_\theta(\eta,\boldsymbol{\alpha}_\diamond)\mathcal{C}_j(\eta)d\eta,\qquad i,j\geq2, \tag{7.31a}$$

$$n^\theta_{i,j}(\boldsymbol{\alpha}_\diamond)=\int_0^\infty\mathcal{C}_i'(\eta)\left[\mathcal{S}_\theta(\eta,\boldsymbol{\alpha}_\diamond)\mathcal{C}_j'(\eta)-\frac{\partial\mathcal{S}_\theta(\eta,\boldsymbol{\alpha}_\diamond)}{\partial\eta}\mathcal{C}_j(\eta)\right]d\eta,\quad i,j\geq2, \tag{7.31b}$$

$$\tilde{s}^\theta_{i,j}(\boldsymbol{\alpha}_\diamond)=\int_0^\infty\mathcal{B}_i(\eta)\mathcal{S}_\theta(\eta,\boldsymbol{\alpha}_\diamond)\mathcal{B}_j(\eta)d\eta,\qquad i,j\geq1. \tag{7.31c}$$

For any eigenfunction v of the Orr-Sommerfeld equation with eigenvalue c it is possible to determine the vorticity ω_p which is the particular solution to the nonhomogeneous Squire equation

$$\left[-\omega_p''+\alpha_\diamond^2\omega_p+\mathrm{i}\mathrm{Re}_\theta\mathcal{S}_\theta(\eta,\boldsymbol{\alpha}_\diamond)\omega_p\right]=\mathrm{i}\mathrm{Re}_\theta[\partial_\eta\mathcal{R}_\theta(\eta,\boldsymbol{\alpha}_\diamond)]v(\eta), \tag{7.32}$$

supplemented by the homogeneous boundary conditions $\omega_p(0)=0$ and $\omega_p(\infty)=0$. This second-order equation once recast in weak form yields the linear algebraic system

$$\left[\tilde{D}^2+\alpha_\diamond^2\tilde{M}+\mathrm{i}\mathrm{Re}_\theta\tilde{S}_\theta(\boldsymbol{\alpha}_\diamond)\right]\boldsymbol{\omega}_p=\mathrm{i}\mathrm{Re}_\theta\boldsymbol{r}(\boldsymbol{\alpha}_\diamond) \tag{7.33}$$

https://doi.org/10.4208/cicp.130411.230911a

with the vector $\boldsymbol{r}$ on the right-hand side defined by

$$r_i(\boldsymbol{\alpha}_\diamond) = \int_0^\infty \mathcal{B}_i(\eta)[\partial_\eta \mathcal{R}_\theta(\eta,\boldsymbol{\alpha}_\diamond)]v(\eta)d\eta. \tag{7.34}$$

The longitudinal and spanwise components $u(\eta)$ and $w(\eta)$ of the velocity associated with the considered eigenfunction $v(\eta)$ can be finally evaluated by solving the two linear systems

$$\tilde{M}\boldsymbol{u} = \mathrm{i}\frac{\alpha\boldsymbol{q}-\beta\boldsymbol{p}}{\alpha^2+\beta^2} \quad \text{and} \quad \tilde{M}\boldsymbol{w} = \mathrm{i}\frac{\beta\boldsymbol{q}-\alpha\boldsymbol{p}}{\alpha^2+\beta^2}, \tag{7.35}$$

where

$$q_i = \int_0^\infty \mathcal{B}_i(\eta)v'(\eta)d\eta \quad \text{and} \quad p_i = \int_0^\infty \mathcal{B}_i(\eta)\omega_p(\eta)d\eta. \tag{7.36}$$

A scaled version of Eqs. (7.25) for the unknowns $\hat{v}(\hat{\eta}) = v(\eta)$ and $\hat{\omega}(\hat{\eta}) = \omega(\eta)$, with $\hat{\eta} = \eta/\chi$, is

$$\begin{cases} \dfrac{1}{\mathrm{Re}_\theta}(\hat{v}'''' - 2\hat{\alpha}_\diamond^2\hat{v}'' + \hat{\alpha}_\diamond^4\hat{v}) - \mathrm{i}\dfrac{\partial}{\partial\hat{\eta}}\left[\chi\mathcal{S}_\theta(\chi\hat{\eta},\hat{\boldsymbol{\alpha}}_\diamond)\hat{v}' - \chi^2\dfrac{\partial\mathcal{S}_\theta(\chi\hat{\eta},\hat{\boldsymbol{\alpha}}_\diamond)}{\partial\eta}\hat{v}\right] \\ \qquad +\mathrm{i}\hat{\alpha}_\diamond^2\chi\mathcal{S}_\theta(\chi\hat{\eta},\hat{\boldsymbol{\alpha}}_\diamond)\hat{v} = \mathrm{i}\hat{c}\hat{\alpha}(-\hat{v}'' + \hat{\alpha}_\diamond^2\hat{v}), \\ \dfrac{1}{\mathrm{Re}_\theta}(-\hat{\omega}'' + \hat{\alpha}_\diamond^2\hat{\omega}) + \mathrm{i}\chi\mathcal{S}_\theta(\chi\hat{\eta},\hat{\boldsymbol{\alpha}}_\diamond)\hat{\omega} = \mathrm{i}\hat{c}\hat{\alpha}\hat{\omega} + \mathrm{i}\chi\dfrac{\partial\mathcal{R}_\theta(\chi\hat{\eta},\hat{\boldsymbol{\alpha}}_\diamond)}{\partial\eta}\hat{v}, \end{cases} \tag{7.37}$$

where $\hat{\boldsymbol{\alpha}}_\diamond = \chi\boldsymbol{\alpha}_\diamond$ and $\hat{c} = \chi c$. The scaled version of the two eigenvalue problems (7.27) will be

$$\hat{A}(\hat{\boldsymbol{\alpha}}_\diamond,\mathrm{Re}_\theta)\hat{\boldsymbol{v}} = \hat{c}B(\hat{\boldsymbol{\alpha}}_\diamond,\mathrm{Re}_\theta)\hat{\boldsymbol{v}}, \qquad \hat{\tilde{A}}(\hat{\boldsymbol{\alpha}}_\diamond,\mathrm{Re}_\theta)\hat{\boldsymbol{\omega}} = \hat{c}\tilde{B}(\hat{\alpha},\mathrm{Re}_\theta)\hat{\boldsymbol{\omega}}, \tag{7.38}$$

where

$$\hat{A}(\hat{\boldsymbol{\alpha}}_\diamond,\mathrm{Re}_\theta) = D^4 + 2\hat{\alpha}_\diamond^2D^2 + \hat{\alpha}_\diamond^4M + \mathrm{i}\mathrm{Re}_\theta\chi\left[\hat{N}_\theta(\hat{\boldsymbol{\alpha}}_\diamond) + \hat{\alpha}_\diamond^2S_\theta(\hat{\boldsymbol{\alpha}}_\diamond)\right], \tag{7.39a}$$

$$\hat{\tilde{A}}(\hat{\boldsymbol{\alpha}}_\diamond,\mathrm{Re}_\theta) = \tilde{D}^2 + \hat{\alpha}_\diamond^2\tilde{M} + \mathrm{i}\mathrm{Re}_\theta\chi\tilde{S}_\theta(\hat{\boldsymbol{\alpha}}_\diamond), \tag{7.39b}$$

with the elements of matrix $\hat{N}_\theta(\hat{\boldsymbol{\alpha}}_\diamond)$ defined by

$$\hat{n}_{i,j}^\theta(\hat{\boldsymbol{\alpha}}_\diamond) = \int_0^\infty \mathcal{C}_i'(\eta)\left[\mathcal{S}_\theta(\eta,\hat{\boldsymbol{\alpha}}_\diamond)\mathcal{C}_j'(\eta) - \chi\frac{\partial\mathcal{S}_\theta(\eta,\hat{\boldsymbol{\alpha}}_\diamond)}{\partial\eta}\mathcal{C}_j(\eta)\right]d\eta, \qquad i,j \geq 2. \tag{7.40}$$

7.4 Results

To test the Orr-Sommerfeld solver for the three-dimensional self-similar boundary layer, the neutral stability curves for three different values of the β_{FS} parameter have been computed, with α_{FS} always set to one, and for different values of the spanwise wave-number β.

In Fig. 6, the curve of neutral stability to 2D perturbation for an accelerating boundary layer with β_{FS}=0.5 is reported. In this case, the favourable pressure gradient has the effect

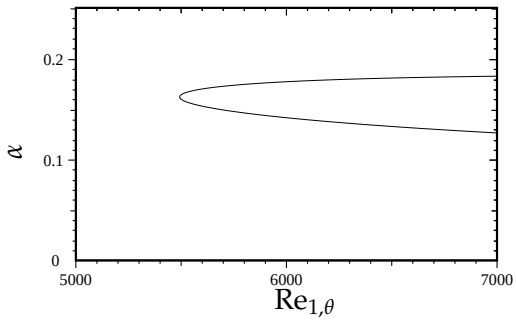

Figure 6: Neutral stability curve of two-dimensional disturbances ($\beta=0$) for $\theta=30°$ for an accelerating Falkner-Skan-Cooke boundary layer with $\alpha_{FS}=1$ and $\beta_{FS}=0.5$.

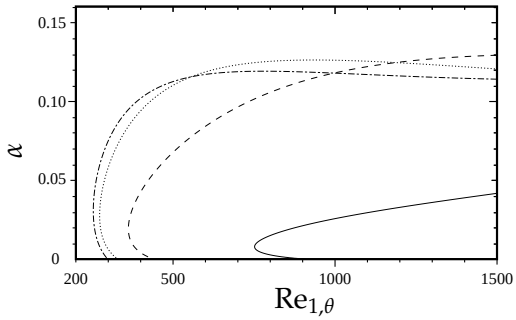

Figure 7: Neutral stability curves of three-dimensional disturbances for $\theta=30°$ for an accelerating Falkner-Skan-Cooke boundary layer with $\alpha_{FS}=1$ and $\beta_{FS}=0.5$. Solid line: $\beta=0.1$. Dashed line: $\beta=0.2$. Dotted line: $\beta=0.3$. Dotted-dashed line: $\beta=0.4$.

of stabilizing the boundary layer moving the critical Reynolds number to a value which is approximately ten times that for the Blasius boundary layer, see, e.g., [8, pp. 226].

When three-dimensional perturbations are considered, the situation changes dramatically. A new branch of the neutral stability curve appears for relatively small α, namely for rather high longitudinal wavelengths, as shown in Fig. 7 where the neutral stability curves for four different values of the spanwise wave-number, $\beta=0.1$, 0.2, 0.3, 0.4, are reported. The unstable perturbations in this case are quasi-two-dimensional spanwise-modulated waves. In the considered interval, the critical Reynolds number diminishes for increasing transversal wavenumbers.

While for an accelerated 3D boundary layer the instability is dominated by spanwise perturbations, the contrary is observed for a decelerating 3D boundary layer, whose neutral curves computed for $\beta_{FS}=-0.1$ are reported in Fig. 8 for $\beta=0$, 0.1, 0.2, 0.3. In this case, the flow is increasingly linearly stable for higher wavenumbers of the transversal perturbation.

When a separated boundary layer is considered, with $\beta_{FS}=-0.1$, the instability domain in the Re-α plane becomes considerably larger as expected, and the critical Reynolds number decreases substantially, as previously found for a 2D separated Falkner-Skan

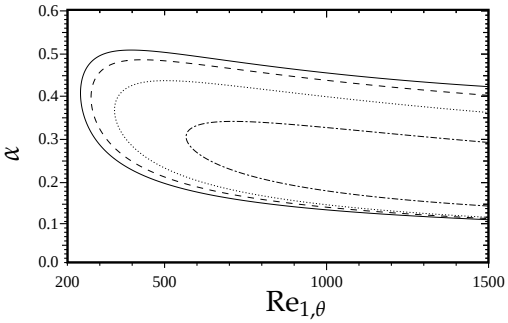

Figure 8: Neutral stability curves of two and three-dimensional disturbances for $\theta=30^\circ$ for a decelerating Falkner-Skan-Cooke boundary layer with $\alpha_{FS}=1$ and $\beta_{FS}=-0.1$. Solid line: $\beta=0$. Dashed line: $\beta=0.1$. Dotted line: $\beta=0.2$. Dotted-dashed line: $\beta=0.3$.

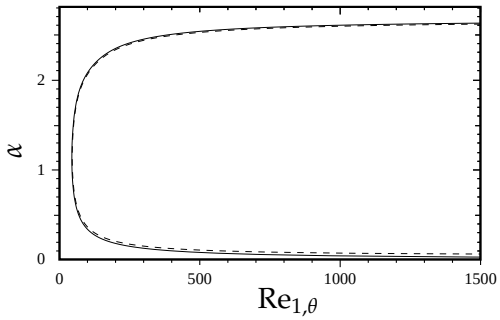

Figure 9: Neutral stability curves of two and three-dimensional disturbances for $\theta=30^\circ$ for a separated Falkner-Skan-Cooke boundary layer with $\alpha_{FS}=1$ and $\beta_{FS}=-0.1$. Solid line: $\beta=0$. Dashed line: $\beta=0.1$.

boundary layer. The neutral stability curves for this case are reported in Fig. 9 for $\beta=0$ and $\beta=0.1$. The neutral stability curve is found to be largely insensitive to the spanwise wavelength of the perturbation.

The eigenfunctions corresponding to the most unstable eigenvalue for $\theta=30^\circ$ for a decelerating nonseparated Falkner-Skan-Cooke boundary layer with $\alpha_{FS}=1$ and $\beta_{FS}=-0.1$, at values $\mathrm{Re}=346$, $\alpha=0.366$, $\beta=0.2$ are reported in Fig. 10.

All the results presented in this section are given only as an example of the power of the proposed spectral method for self-similar boundary layer calculations and they do not pretend to contribute originally to the linear theory of boundary layer stability which is beyond the purpose of the present paper.

8 Conclusions

In this work a new Galerkin spectral solver for the Falkner-Skan equations has been proposed which exploits a suitable basis of Laguerre functions first proposed by Jie Shen for fourth order differential equations on the semi-infinite interval [22]. The Falkner-Skan solver has been completed by a spectral solver for the Cooke equation, governing the self-

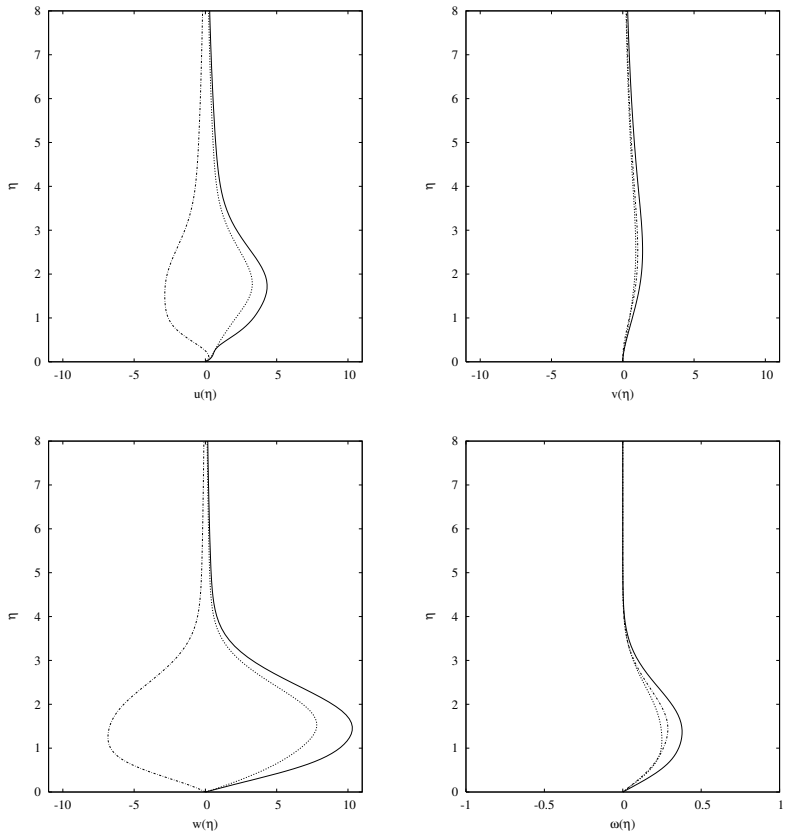

Figure 10: Eigenfunction corresponding to the most unstable eigenvalue for $\theta = 30^\circ$ for a decelerating non-separated Falkner-Skan-Cooke boundary layer with $\alpha_{\mathrm{FS}} = 1$ and $\beta_{\mathrm{FS}} = -0.1$, $\mathrm{Re} = 346$, $\alpha = 0.366$, $\beta = 0.2$. In lexicographic order: u, v, w, ω. Solid line: modulus. Dashed line: real part. Dotted-dashed line: imaginary part.

similar profile of the transversal velocity component, to compute the three-dimensional boundary layer over a flat plate for different values of the external velocity distribution and for different sweep angles. The proposed solver is simple, since the boundary conditions are satisfied by construction in the spectral approximation and the solution algorithm amounts only to matrix multiplications and linear system solutions within a Newton iteration.

The paper addresses also the linear stability of the aforementioned base flow in the parallel approximation by providing a new spectral solver for the Orr-Sommerfeld eigenvalue problem for unconfined boundary layer shear flows. The same algorithmic ingredients of the boundary value solvers are employed to tackle the eigenvalue problem leading to an extremely simple, accurate and stable solver.

All the numerical tests demonstrate the advantages of the proposed numerical techniques to study the linear stability of the considered flows.

Appendix

A Matrices for the biharmonic Laguerre basis

To discretize differential equations over a semi-infinite interval by means of Laguerre polynomials, the matrices representing the derivatives of the unknown variable must be calculated. In this appendix, such matrices are computed in closed form. To this aim we need to express the first and second derivatives of the basis functions in terms of a linear combination of Laguerre polynomials times the exponential function.

Let us now start by considering the first derivative of the basis functions. The derivative of the first two functions can be evaluated directly,

$$\mathcal{C}_0'(x)=-\frac{1}{2}e^{-\frac{x}{2}} \quad \text{and} \quad \mathcal{C}_1'(x)=e^{-\frac{x}{2}}\Big(1-\frac{1}{2}x\Big).$$

For the derivative of the remaining basis functions, with $i\geq 2$, we use the identity $[L_{i-k}^{(k)}(x)]'=-L_{i-k-1}^{(k+1)}(x)$ to compute

$$\begin{aligned}
\mathcal{C}_1'(x)&=\frac{e^{-\frac{x}{2}}}{i(i-1)}\Big\{2xL_{i-2}^{(2)}(x)-\frac{1}{2}x^2L_{i-2}^{(2)}(x)-x^2L_{i-3}^{(3)}(x)\Big\}\\
&=\frac{e^{-\frac{x}{2}}}{i(i-1)}\Big\{2xL_{i-2}^{(2)}(x)-\frac{1}{2}x^2L_{i-2}^{(2)}(x)-x\big[iL_{i-3}^{(2)}(x)-(i-2)L_{i-2}^{(2)}(x)\big]\Big\}\\
&=\frac{e^{-\frac{x}{2}}}{i(i-1)}\Big\{-\frac{1}{2}x^2L_{i-2}^{(2)}(x)-ix\big[L_{i-3}^{(2)}(x)-L_{i-2}^{(2)}(x)\big]\Big\}\\
&=\frac{e^{-\frac{x}{2}}}{i(i-1)}\Big\{-\frac{1}{2}x^2L_{i-2}^{(2)}(x)+ixL_{i-2}^{(1)}(x)\Big\},
\end{aligned}$$

where in the last step the identity $L_{i-3}^{(2)}(x)-L_{i-2}^{(2)}(x)=-L_{i-2}^{(1)}(x)$ has been exploited. The identity (3.4) with $k=1$ is now used to reduce the order of the Laguerre polynomial in the first term to give

$$\begin{aligned}
\mathcal{C}_1'(x)&=\frac{e^{-\frac{x}{2}}}{i(i-1)}\Big\{-\frac{x}{2}\big[iL_{i-2}^{(1)}(x)-(i-1)L_{i-1}^{(1)}(x)\big]+ixL_{i-2}^{(1)}(x)\Big\}\\
&=\frac{e^{-\frac{x}{2}}}{i(i-1)}\frac{x}{2}\Big\{-iL_{i-2}^{(1)}(x)+(i-1)L_{i-1}^{(1)}(x)+2iL_{i-2}^{(1)}(x)\Big\}\\
&=\frac{e^{-\frac{x}{2}}}{2i(i-1)}\Big\{ixL_{i-2}^{(1)}(x)+(i-1)xL_{i-1}^{(1)}(x)\Big\}\\
&=\frac{x^{-\frac{x}{2}}}{2i(i-1)}\Big\{i(i-1)\big[L_{i-2}(x)-L_{i-1}(x)\big]+(i-1)i\big[L_{i-1}(x)-L_i(x)\big]\Big\}\\
&=\frac{e^{-\frac{x}{2}}}{2}\big[L_{i-2}(x)-L_i(x)\big].
\end{aligned}$$

We proceed similarly for the second derivatives. The second derivative of the first two basis functions is

$$\mathcal{C}_0''(x)=\frac{1}{4}e^{-\frac{x}{2}} \quad \text{and} \quad \mathcal{C}_1''(x)=-e^{-\frac{x}{2}}\left(1-\frac{1}{4}x\right).$$

For the other basis functions we obtain

$$\begin{aligned}\mathcal{C}_i''(x)&=\frac{d}{dx}\mathcal{C}_i'(x)=-\frac{e^{-\frac{x}{2}}}{4}\left[L_{i-2}(x)-L_i(x)\right]+\frac{e^{-\frac{x}{2}}}{2}\left[-L_{i-3}^{(1)}(x)+L_{i-1}^{(1)}(x)\right]\\&=\frac{e^{-\frac{x}{2}}}{4}\left[-2L_{i-3}^{(1)}(x)+2L_{i-1}^{(1)}(x)-L_{i-2}^{(0)}(x)+L_i^{(0)}(x)\right].\end{aligned}$$

Thanks to the identity

$$\begin{aligned}L_{i-1}^{(1)}(x)-L_{i-3}^{(1)}(x)&=L_{i-1}^{(1)}(x)-L_{i-2}^{(1)}(x)+L_{i-2}^{(1)}(x)-L_{i-3}^{(1)}(x)\\&=L_{i-1}^{(0)}(x)+L_{i-2}^{(0)}(x)=L_{i-1}(x)+L_{i-2}(x),\end{aligned}$$

we obtain finally

$$\begin{aligned}\mathcal{C}_i''(x)&=\frac{e^{-\frac{x}{2}}}{4}\left[2L_{i-2}(x)+2L_{i-1}(x)-L_{i-2}(x)+L_i(x)\right]\\&=\frac{e^{-\frac{x}{2}}}{4}\left[L_{i-2}(x)+2L_{i-1}(x)+L_i(x)\right].\end{aligned}$$

The basis functions $\mathcal{C}_i(x)$, $i=0,1,2,\cdots$, and their first and second derivatives are collected in the following table:

$\mathcal{C}_0(x)=e^{-\frac{x}{2}}$	$\mathcal{C}_1(x)=xe^{-\frac{x}{2}}$	$\mathcal{C}_i(x)=e^{-\frac{x}{2}}[L_{i-2}(x)-2L_{i-1}(x)+L_i(x)]$
$\mathcal{C}_0'(x)=-\frac{1}{2}e^{-\frac{x}{2}}$	$\mathcal{C}_1'(x)=e^{-\frac{x}{2}}(1-\frac{1}{2}x)$	$\mathcal{C}_i'(x)=\frac{1}{2}e^{-\frac{x}{2}}[L_{i-2}(x)-L_i(x)]$
$\mathcal{C}_0''(x)=\frac{1}{4}e^{-\frac{x}{2}}$	$\mathcal{C}_1''(x)=-e^{-\frac{x}{2}}(1-\frac{1}{4}x)$	$\mathcal{C}_i''(x)=\frac{1}{4}e^{-\frac{x}{2}}[L_{i-2}(x)+2L_{i-1}(x)+L_i(x)]$

where $i\geq 2$.

Once the derivatives of the basis functions have been expressed by means of Laguerre $L_i(x)$ polynomials, it is straightforward to compute the entries of the matrices corresponding to the derivative operators in weak form exploiting the orthogonality relationship

$$\int_0^\infty e^{-x}L_i(x)\,L_j(x)\,dx=\delta_{i,j}, \qquad i,j\geq 0, \tag{A.1}$$

or in the simplest cases, by direct calculation.

A.1 First order derivative matrix

The matrix F representing the first derivative in the considered Laguerre basis has elements defined by

$$f_{i,j}=\int_0^\infty \mathcal{C}_i(x)\mathcal{C}_j'(x)dx, \qquad i,j\geq 0. \tag{A.2}$$

https://doi.org/10.4208/cicp.130411.230911a

Also this matrix is pentadiagonal and is found to be antisymmetric but for the first diagonal element, according to

$$F=\frac{1}{2}\begin{pmatrix} -1 & 1 & 1 & & & & & & \\ -1 & 0 & 1 & -1 & & & & & \\ -1 & -1 & 0 & -2 & 1 & & & & \\ & 1 & 2 & 0 & -2 & 1 & & & \\ & & -1 & 2 & 0 & \ddots & \ddots & & \\ & & & -1 & \ddots & \ddots & \ddots & 1 & \\ & & & & \ddots & \ddots & 0 & -2 & 1 \\ & & & & & -1 & 2 & 0 & -2 \\ & & & & & & -1 & 2 & 0 \end{pmatrix}. \tag{A.3}$$

A.2 Second order derivative (stiffness) matrix

The second order stiffness matrix $S=D^2$, after integration by parts, has elements defined by

$$s_{i,j}=\int_0^\infty C_i'(x)C_j'(x)dx, \qquad i,j\geq 0. \tag{A.4}$$

This matrix is again symmetric and always pentadiagonal, its entries being

$$D^2=\frac{1}{4}\begin{pmatrix} 1 & -1 & -1 & & & & & & \\ -1 & 2 & 1 & 1 & & & & & \\ -1 & 1 & 2 & 0 & -1 & & & & \\ & 1 & 0 & 2 & 0 & -1 & & & \\ & & -1 & 0 & 2 & \ddots & \ddots & & \\ & & & -1 & \ddots & \ddots & \ddots & -1 & \\ & & & & \ddots & \ddots & \ddots & 0 & -1 \\ & & & & & -1 & 0 & 2 & 0 \\ & & & & & & -1 & 0 & 2 \end{pmatrix}. \tag{A.5}$$

A.3 Third order derivative matrix

The elements of the matrix corresponding to the weak third order derivative are, after integration by parts,

$$t_{i,j}=\int_0^\infty C_i'(x)C_j''(x)dx, \qquad i,j\geq 0. \tag{A.6}$$

The profile of T is still pentadiagonal and its entries are found to be

$$T=\frac{1}{8}\begin{pmatrix} -1 & 3 & -1 & & & & & \\ 1 & -4 & 3 & 1 & & & & \\ 1 & -3 & 0 & -2 & -1 & & & \\ & -1 & 2 & 0 & -2 & -1 & & \\ & & 1 & 2 & \ddots & \ddots & \ddots & \\ & & & 1 & \ddots & \ddots & -2 & -1 \\ & & & & \ddots & 2 & 0 & -2 \\ & & & & & 1 & 2 & 0 \end{pmatrix}. \tag{A.7}$$

A.4 Fourth order derivative matrix

The elements of matrix $Q=D^4$ of the fourth order derivative, after two successive integrations by parts, are defined by

$$q_{i,j}=\int_0^\infty \mathcal{C}_i''(x)\mathcal{C}_j''(x)\,dx, \qquad i,j\geq 0. \tag{A.8}$$

The pentadiagonal symmetric matrix D^4 has entries

$$D^4=\frac{1}{16}\begin{pmatrix} 1 & -3 & 1 & & & & & & \\ -3 & 10 & -5 & -1 & & & & & \\ 1 & -5 & 6 & 4 & 1 & & & & \\ & -1 & 4 & 6 & 4 & 1 & & & \\ & & 1 & 4 & 6 & \ddots & \ddots & & \\ & & & 1 & \ddots & \ddots & \ddots & 1 & \\ & & & & \ddots & \ddots & \ddots & 4 & 1 \\ & & & & & 1 & 4 & 6 & 4 \\ & & & & & & 1 & 4 & 6 \end{pmatrix}. \tag{A.9}$$

A.5 Mass matrix

The mass matrix M with elements

$$m_{i,j}=\int_0^\infty \mathcal{C}_i(x)\mathcal{C}_j(x)\,dx, \qquad i,j\geq 0, \tag{A.10}$$

https://doi.org/10.4208/cicp.130411.230911a

is symmetric and is found to be pentadiagonal, with the following entries:

$$M=\begin{pmatrix} 1 & 1 & 1 & & & & & & \\ 1 & 2 & 3 & -1 & & & & & \\ 1 & 3 & 6 & -4 & 1 & & & & \\ & -1 & -4 & 6 & -4 & 1 & & & \\ & & 1 & -4 & 6 & \ddots & \ddots & & \\ & & & 1 & \ddots & \ddots & \ddots & 1 & \\ & & & & \ddots & \ddots & \ddots & -4 & 1 \\ & & & & & 1 & -4 & 6 & -4 \\ & & & & & & 1 & -4 & 6 \end{pmatrix}. \tag{A.11}$$

A.6 Matrices for the harmonic basis

For completeness we give the matrix $\tilde{D}^2$ of the second order derivative, after integration by parts, and the mass matrix $\tilde{M}$ associated with the basis

$$\mathcal{B}_0(\eta)\equiv e^{-\frac{\eta}{2}} \quad \text{and} \quad \mathcal{B}_i(\eta)\equiv\frac{\eta e^{-\frac{\eta}{2}}L_{i-1}^{(1)}(\eta)}{i}, \quad \text{for } i\geq 1. \tag{A.12}$$

The elements of the matrices are defined respectively by

$$\tilde{d}^2_{i,j}=\int_0^\infty \mathcal{B}_i'(\eta)\mathcal{B}_j'(\eta)d\eta \quad \text{and} \quad \tilde{m}_{i,j}=\int_0^\infty \mathcal{B}_i(\eta)\mathcal{B}_j(\eta)d\eta, \quad \text{for } i,j\geq 0.$$

Both matrices are symmetric tridiagonal and are as follows:

$$\tilde{D}^2=\frac{1}{4}\begin{pmatrix} 1 & -1 & & & & \\ -1 & 2 & 1 & & & \\ & 1 & 2 & 1 & & \\ & & 1 & \ddots & \ddots & \\ & & & \ddots & \ddots & 1 \\ & & & & 1 & 2 \end{pmatrix} \quad \text{and} \quad \tilde{M}=\begin{pmatrix} 1 & 1 & & & & \\ 1 & 2 & -1 & & & \\ & -1 & 2 & -1 & & \\ & & -1 & \ddots & \ddots & \\ & & & \ddots & \ddots & -1 \\ & & & & -1 & 2 \end{pmatrix}. \tag{A.13}$$

References

[1] A. Asaithambi, A second order finite-difference method for the Falkner-Skan equation, Appl. Math. Comput., 156 (2004), 779–786.
[2] A. Asaithambi, Numerical solution of the Falkner-Skan equation using piecewise linear functions, Appl. Math. Comput., 159 (2004), 267–273.

[3] A. Asaithambi, Solution of the Falkner-Skan equations by recursive evaluation of Taylor coefficients, J. Comput. Appl. Math., 176 (2005), 203–214.
[4] J. P. Boyd, Orthogonal rational functions on a semi-infinite interval, J. Comput. Phys., 70 (1987), 63–88.
[5] T. Cebeci and H. B. Keller, Shooting and parallel shooting methods for solving the Falkner-Skan boundary-layer equation, J. Comput. Phys., 7 (1971), 289–300.
[6] J. C. Cooke, The boundary layer of a class of infinite yawed cylinders, Math. Proc. Cambridge Philos. Soc., 46 (1950), 645–648.
[7] A. Dobrinsky, Adjoint Analysis for Receptivity Prediction, Ph.D. Thesis, Rice University, Houston, 2002.
[8] P. G. Drazin and W. H. Reid, Hydrodynamics Stability, Cambridge University Press, New York, 1981.
[9] V. M. Falkner and S. W. Skan, Some approximate solutions of the boundary layer equations, Philos. Mag., 12 (1931), 865–896.
[10] R. Fazio, The Blasius problem formulated as a free boundary value problem, Acta Mech., 95 (1992), 1–7.
[11] T. M. Fischer, A Galerkin approximation for linear eigenvalue problems in two and three-dimensional boundary layer flows, Lect. Notes Math., 1431 (1990), 100–108.
[12] W. H. Hager, Blasius: a life in research and education, Exp. Fluids, 34 (2003), 566–571.
[13] D. R. Hartree, On an equation occurring in Falkner and Skan's approximate treatment of the equations of the boundary layer, Proc. Cambridge Philos. Soc., 33 (1937), 223–239.
[14] R. S. Heeg, D. Dijkstra and P. J. Zandbergen, The stability of Falkner-Skan flows with several inflection points, ZAMP, 50 (1999), 82–93.
[15] L. M. Mack, Boundary layer linear stability theory, in Special course on stability and transition of laminar flow, AGARD Report No. 709, 1984.
[16] R. E. Meyer, Introduction to Mathematical Fluid Dynamics, Wiley, New York, 1971.
[17] K. Parand, M. Shahini and M. Dehghan, Solution of a laminar boundary layer via a numerical method, Commun. Nonlinear Sci. Numer. Simulat., 15 (2010), 360–367.
[18] K. Parand and A. Taghavi, Rational scaled generalized Laguerre function collocation method for solving the Blasius equation, J. Comput. Appl. Math., 233 (2009), 980–989.
[19] A. A. Salama, Higher order method for solving free boundary problems, Numer. Heat Trans. B Fundament., 45 (2004), 385–394.
[20] H. Schlichting and K. Gersten, Boundary Layer Theory, Springer-Verlag, Berlin, 2000.
[21] P. J. Schmid and D. S. Henningson, Stability and Transition in Shear Flows, Springer-Verlag, New York, 2001.
[22] J. Shen, Stable and efficient spectral methods in unbounded domains using Laguerre functions, SIAM J. Numer. Anal., 38 (2000), 1113–1133.
[23] J. Shen and L. L. Wang, Some recent advances on spectral methods for unbounded domains, Commun. Comput. Phys., 5 (2009), 195–241.
[24] J. Zhang and B. Chen, An iterative method for solving the Falkner-Skan equation, Appl. Numer. Math., 210 (2009), 215–222.